Frontiers of Environmental Science & Engineering
2025, 19(4): 48 https://doi.org/10.1007/s11783-025-1968-9

RESEARCH ARTICLE

Evaluation of the halogenation and photofate of the blood pressure regulator losartan in water: reactivity and mechanisms

Linke Jiang[1], Yong Li[2], Shuiqin Shi[1], Junmei Yan[1], Lianbao Chi ✉ [3], Hui Liu[4], Mingbao Feng ✉ [1]

1. Fujian Key Laboratory of Coastal Pollution Prevention and Control, College of the Environment & Ecology, Xiamen University, Xiamen 361102, China
2. Guangzhou Hexin Instrument Co., Ltd., Guangzhou 510530, China
3. CAS Key Laboratory of Marine Ecology and Environmental Sciences, Institute of Oceanology, Chinese Academy of Sciences, Qingdao 266071, China
4. College of Biological, Chemical Sciences and Engineering, Jiaxing University, Jiaxing 314001, China

HIGHLIGHTS

- Losartan showed distinct reactivity with multiple chemical oxidants.
- Mechanisms of losartan via chlorination, bromination, and photolysis were explored.
- Direct and indirect photolysis contributed differently to losartan photolysis.
- The transformation products remained certain environmental risks.

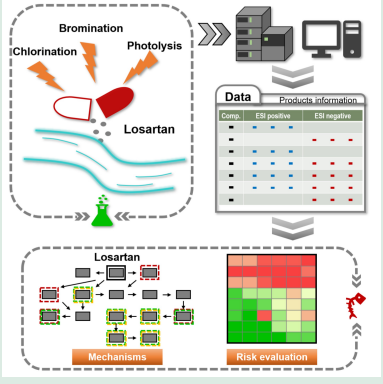

ABSTRACT: Chlorinating wastewater before it is released into surface water can change the fate of organic pollutants. This transformation is influenced by chlorine residues, bromine-containing wastewater, and solar radiation. Losartan (LOS), one of the earliest sartan antihypertensive drugs produced, is used worldwide and has been found in the environment. However, its transformation mechanisms and environmental risks have not been systematically investigated. This research presents the degradation kinetics, transformation products, and environmental risks of LOS in different scenarios. The results revealed that $k_{app,\ HClO\ (LOS)}$ ranged from 0.47 to 8.30 L/(mol·s) at pH 5.0–8.0. The $k_{app,\ HBrO\ (LOS)}$ values at pH 5.0–8.0 ranged from 8.38×10^3 to 1.55×10^5 L/(mol·s), revealing a faster bromination reaction than chlorination. LOS degrades through direct photolysis, carbonate radicals ($CO_3^{\bullet-}$), and singlet oxygen ($^1O_2$) under sunlight exposure. The solar/chlorination process accelerates the reaction rate through radical activity. In addition, chlorination and bromination resulted in halogen addition to the aromatic ring, whereas hydroxylation, hydrogen abstraction, demethylation, ring opening, and hydrolysis reactions were observed across all processes. Some products exhibit high biodegradation resistance and high toxicity, potentially threatening the aquatic environment. This study aims to enhance our understanding of the environmental behavior and resulting risks of LOS by exploring its environmental

✉ Corresponding authors. E-mails: chilianbao@qdio.ac.cn (L. Chi); mfeng24@xmu.edu.cn (M. Feng)
Article history: Received 7 September 2024, Revised 9 December 2024, Accepted 7 January 2025, Available online 20 February 2025

fate through various transformation processes.

KEYWORDS: Chlorination, Blood pressure regulator, Kinetics, Photolysis, Reaction mechanisms

1 Introduction

Losartan (LOS) is an angiotensin II receptor blocker that reduces blood pressure by causing vasodilation through blocking the binding of angiotensin II to receptors in blood vessels. It is widely manufactured and used globally as a pharmaceutical and personal care product (PPCP) (Meyer et al., 2019). LOS is a commonly prescribed medication for treating high blood pressure, with 52 million prescriptions issued in the US in 2017 (Martínez-Pachón et al., 2021; Li et al., 2023). However, the extensive use of LOS has led to its presence in the environment. For example, LOS has been detected in influent samples from wastewater treatment plants at concentrations between 0.50 and 2.18 μg/L (Oosterhuis et al., 2013; Martínez-Pachón et al., 2021), with a yearly average concentration of 26.85 μg/L in hospital effluents (Becker et al., 2023). Contamination by LOS was observed in three out of four Brazilian beaches, with the highest concentration recorded at 548.0 ng/L. Studies have shown that LOS poses a high toxicity risk to crustaceans and a moderate risk to fish (Roveri et al., 2020). Various assessments have categorized LOS as a pollutant with moderate to high risk on the basis of indices such as the risk quotient (RQ), optimized RQ_f, and toxic units (Ofrydopoulou et al., 2021). Additionally, LOS may be transformed into more harmful compounds via electrochemical oxidation, heat-activated persulfate, and chlorination processes, as predicted by acute, chronic, and developmental toxicity (Soares et al., 2017; Ioannidi et al., 2022; Ofrydopoulou et al., 2022), highlighting the necessity of research on LOS degradation.

Chlorination is a common method used in wastewater treatment plants for disinfecting effluents. It interacts with other variables to influence various processes. Bromide-containing wastewater or natural water may produce HBrO and BrO^- when chlorinated with free available chlorine (FAC) (Liu et al., 2019; Rose et al., 2020; Hu et al., 2021). The solar/chlorine system is commonly employed for wastewater treatment and pollutant degradation under sunlight irradiation (Shu et al., 2014; Hua et al., 2019; Lee et al., 2020). When wastewater effluents enter surface waters, photoproduced reactive intermediates (PPRIs), such as hydroxyl radicals ($^{\bullet}OH$), indirectly aid in pollutant breakdown due to the intricate interplay between sunlight and water (Lai et al., 2020; Pozdnyakov et al., 2020; Li et al., 2023). The combination of FAC usage, Br^- presence, and the joint effects of sunlight and PPRIs can result in the formation of specific products, such as methylparaben, trihalomethanes and haloacetic acid, during pollutant degradation (Young et al., 2018; Abdallah et al., 2021).

However, current research on the multi-pathway transformation of LOS is limited. Despite some studies examining the degradation of LOS through various processes, such as UV photolysis, UV/H_2O_2, and UV/persulfate, the simultaneous use of different processes and their impact on the toxicity of transformation products have not been extensively studied (Ali et al., 2023). There is a paucity of research on the impact of photolysis, both direct and indirect, on LOS degradation. Insights into the degradation mechanisms and associated risks are scarce. A critical toxicity assessment comparing LOS transformation products with their parent compounds is urgently needed to address the potential environmental risks.

To address this gap, this study focused on LOS, an antihypertensive drug that is found in natural water bodies worldwide, with the following objectives: (1) to elucidate the reaction kinetics of LOS with FAC and bromine and under photolysis-related environmental processes (direct photolysis and reactivity with different PPRIs), (2) to identify the TPs generated from LOS degradation and unveil the transformation mechanisms in different reaction systems, and (3) to evaluate the transformation-derived risks of LOS using computer-based toxicity prediction software. Furthermore, this research employs a multidisciplinary approach that combines environmental chemistry, toxicology, and computational chemistry to provide a comprehensive assessment of the environmental impact of LOS. Overall, this research has broad significance for comprehending the degradation fate and behavior of LOS under various conditions, including chlorine-based disinfection units and sunlit freshwater systems.

2 Materials and methods

2.1 Reagents and chemicals

Losartan (LOS, 98%) was obtained from Rhawn Co., Ltd. (Shanghai, China). L-tyrosine (Tyr, 99%), pyridine (Pyr, 99%), sodium thiosulfate pentahydrate (> 98%),

sodium hydroxide (NaOH, ⩾ 98%), potassium bromide (KBr, 99%), sodium bicarbonate ($NaHCO_3$, ⩾ 99.8%), hydrogen peroxide solution (H_2O_2, 30%), and methanol (HPLC grade) were supplied by Macklin Co., Ltd. (Shanghai, China). Sodium hypochlorite (NaClO, 4.00%–4.99%), furfuryl alcohol (FFA, 98%), rose bengal (RB, 95%), and sodium anthraquinone-2-sulfonate (AQ2S, ⩾ 98%) were purchased from Sigma-Aldrich Co., Ltd. (Shanghai, China). Sodium nitrate ($NaNO_3$, ⩾ 99%) was supplied by Xilong Chemical Co., Ltd. (Guangzhou, China). *p*-Nitrophenyl (PNA, 98%) was purchased from Aladdin Biochemical Technology Co., Ltd. (Shanghai, China). Additionally, 18.0 MΩ-cm Milli-Q water (Beijing, China) was used to obtain the reaction solutions.

2.2 Chlorination and bromination of LOS

In the LOS chlorination experiment, excess FAC ($[FAC]_0 > 10\ [LOS]_0$) was used to create pseudo-first-order kinetic conditions, and a 10.0-mmol/L Na_2HPO_4 solution was used to buffer the reaction pH. The chlorination experiments were conducted in 50.0 mL glass beakers at pH 5.0–8.0. First, 100.0–300.0 μmol/L FAC was added to 20.0 mL of LOS solution (5.0 μmol/L). Specifically, 1.0 mL samples were transferred into high-performance liquid chromatography (HPLC) vials containing sodium thiosulfate as a quencher (0.1 mol/L) for measurement via HPLC. The second-order rate constants are listed in Text S1.

For the bromination of LOS, the second-order rate constants were measured via a competitive kinetic approach considering its high reactivity. The reference chemical MeP reacted adequately after 12 h with LOS via bromination at a concentration of 5.0 μmol/L at pH 5.0–8.0. Different concentrations of oxidant (0.25–5.0 μmol/L) were added to the system, the reaction was complete, and then the samples were transferred into HPLC vials for measurement. The main equations are shown in Eqs. (1)–(3). $k_{app,\ HBrO}$ was determined on the basis of the retention rates of the two substances, and the calculation processes are described in Text S1.

$$LOS + HBrO \xrightarrow{k_{app,\ HBrO\ (LOS)}} products, \quad (1)$$

$$MeP + HBrO \xrightarrow{kapp,HBrO(MeP)} products, \quad (2)$$

$$\ln\frac{[LOS]_{T,0}}{[LOS]_{T,t}} = \frac{k_{app,\ HBrO\ (LOS)}}{k_{app,\ HBrO\ (MeP)}} \ln\frac{[MeP]_{T,0}}{[MeP]_{T,t}}. \quad (3)$$

$k_{app,\ HBrO\ (LOS)}$ and $k_{app,\ HBrO\ (MeP)}$ are the second-order rate constants of LOS and MeP at pH 5.0–8.0 in the bromination reactions. The values of $k_{app\ HBrO\ (MeP)}$ at different pH values were obtained from the literature (Abdallah et al., 2021), and the $k_{app,\ HBrO\ (LOS)}$ values at different pH values are shown in Texts S1.

2.3 Photodegradation experiments

To systematically evaluate the photodegradation effect, both direct and indirect photolysis experiments were conducted using a sunlight simulator (BL-GHX-V, BILON, China) at wavelengths from 290 to 800 nm, as well as a xenon arc lamp (BL-GHC-Xe-300, BILON, China). The photodegradation experiments were performed in 50.0 mL beakers containing 5.0 μmol/L LOS. The direct photolysis quantum yield was evaluated via *p*-nitrophenyl (PNA)/pyridine photometry in the direct photolysis experiments. The indirect photolysis experiments were performed with the photoinduced reactive species $^{\bullet}OH$, $CO_3^{\bullet -}$, $^1O_2$, and AQ2S, and the detailed descriptions are shown in Text S2 (Ouyang et al., 2023; Shang et al., 2023; Wang et al., 2024). To model the photoinduced transformation kinetics of LOS in surface water and determine the contributions of direct and indirect photolysis, the software tool Aqueous Photochemistry of Environmentally Occurring Xenobiotics (APEX) was employed (Bodrato and Vione, 2014). The LOS data and water quality parameters were set as inputs in APEX to calculate the predicted LOS half-life and fraction of LOS degradation at a water depth of 0.5 m.

The performance of the solar/chlorine system with regard to degrading LOS (5.0 μmol/L) was measured in a phosphate buffer solution at pH 7.0 to account for the presence of both chlorine and solar irradiation in discharged wastewater. The detailed sampling and determination procedures were the same as those for the above chlorination and photolysis experiments (Text S2).

2.4 Analytical procedures

The residual concentrations of LOS and related reference chemicals were quantitively determined using HPLC (Shimadzu LC-20AD) with a diode array detector and autosampler. Different compounds have specific mobile phase ratios for chromatographic separation and determination. To investigate LOS transformation, solid-phase extraction (SPE) was conducted prior to product analysis (Text S3). The TPs associated with LOS degradation were identified via an Agilent 1260 Infinity HPLC and an AB Sciex hybrid quadrupole time-of-flight mass spectrometer (LCMS-Triple TOF 5600). The toxicity, biodegradability index, and predicted endocrine-disrupting effects of LOS and

its TPs were evaluated. ChemDraw Ultra 12.0 (ChemDraw) was utilized to generate the chemical structures of LOS and its TPs and obtain their SMILES codes to predict toxicity. CompTox software was subsequently used to assess developmental toxicity, mutagenicity, and endocrine-disrupting effects. The prediction of biodegradability, as well as acute/chronic aquatic toxicity, of LOS and its TPs were determined individually by BioWin5 and ECOSAR from the EPI Suite™ (EPI Suite™-Estimation Program Interface | US EPA). The EDC-predictor strategy was used to predict possible endocrine-disrupting mechanisms of TPs produced from LOS degradation.

3 Results and discussion

3.1 Chlorination and bromination kinetics of LOS

In this section, we measured the pH-dependent second-order rate constants of the reaction between LOS and FAC ($k_{app,\ HClO\ (LOS)}$) under pseudo-first-order conditions within the pH range of 5.0 to 8.0. The pseudo-first-order rate constants for LOS ($k_{obs,\ HClO}$) were determined by conducting reactions with varying concentrations of FAC. The results in Fig. S1 demonstrate a strong correlation coefficient (R^2 = 0.9842–0.9888), indicating that the experimental reaction with LOS follows first-order kinetics. Similarly, on the basis of the data obtained at different FAC concentrations, the reaction with FAC also exhibited first-order kinetics. Therefore, the overall reaction is a second-order reaction. The measured $k_{app,\ HClO\ (LOS)}$ values ranged from 0.47 to 8.30 L/(mol·s) at pH 5.0–8.0, as shown in Fig. 1(A). Furthermore, with decreasing pH, an increasing trend in the reactivity between LOS and FAC was observed. For chlorination experiments, NaClO solution was utilized as the source of FAC, and the reaction proceeded as follows: $NaClO + H_2O \Leftrightarrow NaOH + HClO$. An acidic environment promotes the formation of HClO, and at low pH, $[H^+]$ is elevated, resulting in enhanced oxidation properties ($HClO + H^+ + 2e^- \Leftrightarrow Cl^- + H_2O$) (Jiang and Lloyd, 2002). In contrast, the reactions between ClO^- and LOS^- were negligible because ClO^- is less oxidizing than HClO is (Li et al., 2023). Equations (4) and (5) can be utilized to establish reaction kinetic models to evaluate $k_{app,\ HClO\ (LOS)}$, as depicted in Fig. 1(A). The calculated k values for each reaction step are outlined in Table 1. The details of the derivation process are shown in Eqs. (6)–(9) and Text S2.

When wastewater containing bromide is treated with chlorine, it may produce BrO^- and HBrO. BrO^- has a much greater oxidation ability than does chlorine (Abdallah et al., 2021). In this study, BrO^- was formed according to the equation $ClO^- + Br^- \Leftrightarrow BrO^- + Cl^-$ (Lei et al., 2004). Figure S2 displays the linear correlations observed in the bromination experiments (R^2 = 0.9805–0.9884), and the second-order rate constant of LOS ($k_{app,\ HBrO\ (LOS)}$) was calculated to be 8.38 × 10^3–1.55 × 10^5 L/(mol·s) at pH 5–8, significantly exceeding the values for $k_{app,\ HClO\ (LOS)}$. In contrast to chlorination, the value of $k_{app,\ HBrO\ (LOS)}$ increased with pH due to the increase in $[BrO^-]$ and the reactivity between BrO^- and LOS^-; this trend was consistent with that in a previous study at pH 5–9 with 0–15 μmol/L bromine (Abdallah et al., 2015). The fitted parameters are listed in Table 1 and were evaluated according to Eqs. (4)–(9):

$$-\mathrm{d}[\mathrm{LOS}]_T/\mathrm{dt} = k_{app,\ HOX}[\mathrm{HOX}][\mathrm{LOS}]_T \quad (4)$$

$$k_{app,\ HOX} = k_1\alpha_1\beta_1 + k_2\alpha_2\beta_1 + k_3\alpha_1\beta_2 + k_4\alpha_2\beta_2, \quad (5)$$

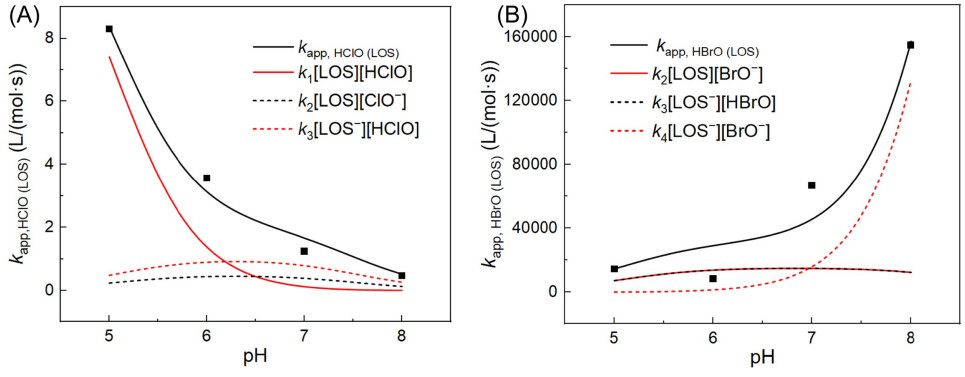

Fig. 1 The second-order rate constants (k_{app}) fitting of pH and LOS degraded by oxidants (i.e., (A) FAC, (B) HBrO.

Table 1 Relevant reactions for chlorination and bromination of LOS

Reactions	Chlorination		Bromination	
	Kinetics constants	Value	Kinetics constants	Value
$HOX \Leftrightarrow H^+ + XO^-$	$pK_{a,\,HOCl}$	7.54	$pK_{a,\,HOBr}$	8.62
$LOS \Leftrightarrow H^+ + LOS^-$	$pK_{a,\,LOS}$	4.26	$pK_{a,\,LOS}$	4.26
$LOS + HXO \overset{k_1}{\Rightarrow}$ products	k_1	14.09 L/(mol·s)	k_1	Negligible
$LOS + XO^- \overset{k_2}{\Rightarrow}$ products	k_2	155.63 L/(mol·s)	k_2	5.72×10^7 L/(mol·s)
$LOS^- + HXO \overset{k_3}{\Rightarrow}$ products	k_3	1.50 L/(mol·s)	k_3	1.54×10^4 L/(mol·s)
$LOS^- + XO^- \overset{k_4}{\Rightarrow}$ products	k_4	Negligible	k_4	6.86×10^5 L/(mol·s)

$$\alpha_1 = [H^+]/([H^+] + K_{a,\,LOS}), \quad (6)$$

$$\alpha_2 = K_{a,\,LOS}/([H^+] + K_{a,\,LOS}), \quad (7)$$

$$\beta_1 = [H^+]/([H^+] + K_{a,\,HOX}), \quad (8)$$

$$\beta_2 = K_{a,\,HOX}/([H^+] + K_{a,\,HOX}). \quad (9)$$

The measured k_{app} values at pH 5.0–8.0 were analyzed via nonlinear least squares regression. The regression results were used to estimate k_{app} for the basic reactions listed in Table 1. Figure 1 indicates that the predicted k_{app} values of both oxidation systems matched the observed k_{app} values within tolerance. This suggested that the elemental reactions in Table 1 are sufficient for explaining the chlorination/bromination reactions. The k_4 of chlorination and the k_1 of bromination were negligible because of the reactivity between LOS/LOS^- and halogens. Furthermore, the values of $k_{app,\,HClO\,(LOS)}$ were slightly lower than those reported in other studies, in which the $k_{app,\,HClO}$ values ranged from 0.21 to 160 L/(mol·s) at pH 5.0–9.0 (Qin et al., 2014; Wu et al., 2016; Li et al., 2023). These results indicated the recalcitrance of LOS during chlorination. For bromination experiments, the measured $k_{app,\,HBrO}$ values reported in other studies ranged from 74.0 to 1.03×10^7 L/(mol·s) at pH 3.0–11.0 (Acero et al., 2013; Abdallah et al., 2015; Li et al., 2015). The measured $k_{app,\,HBrO\,(LOS)}$ values are within this range, indicating that bromination is more reactive than chlorination.

3.2 Reactivity of LOS during solar photodegradation

The photodegradation experiments were divided into direct and indirect photolysis experiments. By using SSL, $^{\bullet}OH$, $CO_3^{\bullet-}$, $^1O_2$, and $^3CDOM^*$, we estimated the photochemical parameters Φ_{LOS}, $k'_{LOS,\,^{\bullet}OH}$, $k_{LOS,\,CO_3^{\bullet-}}$, $k_{LOS,\,^1O_2}$, and $k_{^3AQ2S^*,\,LOS}$, as shown in Table 2. Eventually, the photodegradation kinetics of LOS were fitted under simulated natural water conditions by APEX software with a day–night cycle (Figs. 2 and 3).

Table 2 Reactivity of photolysis (direct photolysis quantum yields and k_{app}) of LOS

Photolysis constants	LOS
Φ_{LOS} (unitless)	1.10×10^{-6}
$k_{LOS,\,^{\bullet}OH}$ (L/(mol·s))	1.76×10^7
$k_{LOS,CO_3^{\bullet-}}$ (L/(mol·s))	2.89×10^7
$k_{LOS,\,^1O_2}$ (L/(mol·s))	9.36×10^7
$k_{LOS,\,^3AQ2S^*}$ (L/(mol·s))	2.04×10^7

To understand how LOS degrades in surface water, the direct photolysis quantum yield of LOS (Φ_{LOS}) was measured at pH 7.0 to be 1.10×10^{-6}. This observed value is less than those reported in previous studies on the direct photolysis of sulfamethoxazole, sulfamethazine, sulfadiazine, and trimethoprim. The k values ranged from 4.53×10^{-6} to 2.97×10^{-2} at pH 7.0–7.8 (Liu and Williams, 2007; Baeza and Knappe, 2011; Lastre-Acosta et al., 2019), confirming that LOS is difficult to degrade by direct photolysis. $^{\bullet}OH$ can degrade pollutants in natural water and effectively oxidize organic compounds generated by exposing H_2O_2 to UV light at pH 7.0. From the experiments, the value of $k'_{LOS,\,^{\bullet}OH}$ was calculated to be 1.76×10^7 L/(mol·s), which is less than those for bisphenol-A, 17-α-estradiol, and isoxazole degradation reported in previous studies (Rosenfeldt and Linden, 2004; Ling et al., 2016; Russo et al., 2020; Zhang and Huang, 2020). Figure 2(B) shows a low contribution of $^{\bullet}OH$ in natural water, likely because $^{\bullet}OH$ can react with DOM more readily than LOS can. At pH 7.0, the LOS solution was exposed to SSL with CO_3^{2-}/HCO_3^- to create $CO_3^{\bullet-}$ because of the presence of CO_3^{2-}/HCO_3^- in surface water. From the experiments, the value of $k_{LOS,CO_3^{\bullet-}}$ was measured to be 2.89×10^7 L/(mol·s) at pH 7.0, which is similar to the reported range of 2.09×10^6 to 5.20×10^8

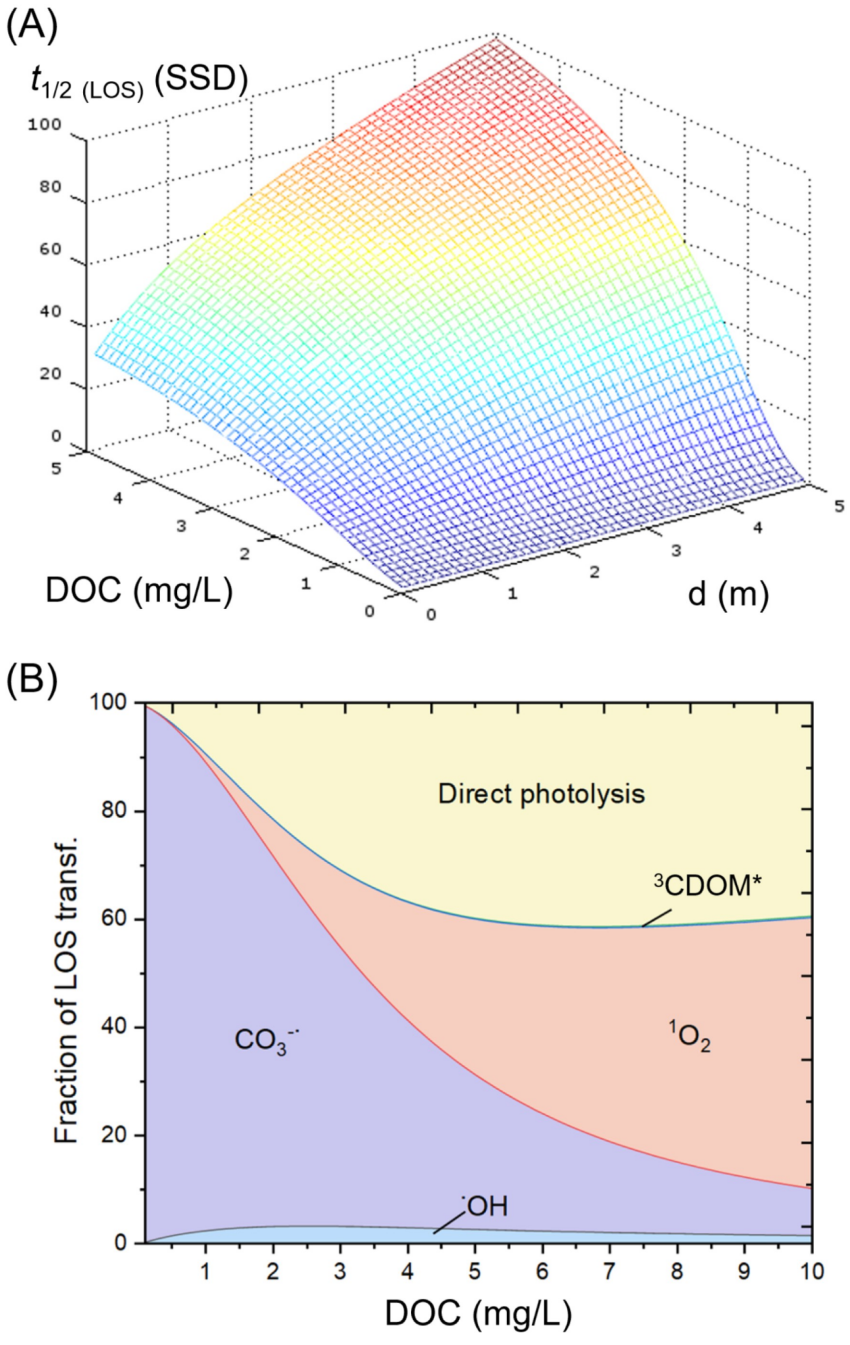

Fig. 2 (A) Estimation of photodegradation half-lives of LOS as a function of the DOC and water depth d by APEX. Conditions: 0.1 mmol/L nitrate, 1.0 mmol/L bicarbonate, 10.0 μmol/L carbonate, SSD (summer sunny days), (B) The contributions of different photoinduced pathways to LOS photolysis predicted by APEX. Conditions: 0.5 m depth, 0.1 mmol/L nitrate, 1.0 μmol/L nitrite, 1.0 mmol/L bicarbonate, 10.0 μmol/L carbonate, SSD, pH 7.0.

L/(mol·s) for the degradation of nitrogen or halogen-containing compounds at pH 6.0–8.6 (Zhou et al., 2020; Carena et al., 2022; Xu et al., 2023). $CO_3^{\bullet-}$ is significant after the photodegradation of LOS, as depicted in Fig. 2(B), because of its elevated reactivity and abundance in surface water (Hao et al., 2020). The reactivities of $^1O_2$ and LOS can be evaluated by adding RB to yield $^1O_2$. The measured value of $k_{LOS,\,^1O_2}$ was 9.36×10^7 L/(mol·s), suggesting that LOS degradation was more prominent than direct photolysis and the

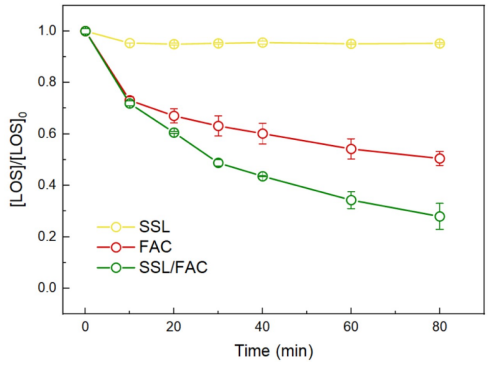

Fig. 3 Removal of LOS by direct photolysis, chlorination, and solar/chlorine system in phosphate buffer solution. Conditions: $[LOS]_0$ = 5.0 μmol $[FAC]_0$ = 100.0 μmol, xenon arc lamp intensity = 300 W/m^2, pH 7.0.

$CO_3^{\bullet-}$ reaction (Fig. 2(B)). Additionally, the triplet state of chromophoric dissolved organic matter (^{3}CDOM*) in natural water can also contribute to the photodegradation of LOS. In this study, AQ2S was used as a representative of CDOM, and it was found that 3CDOM* was not the primary reactive substance in LOS photodegradation. $k_{^3AQ2S^*, LOS}$ was calculated to be 2.04 × 10^7 L/(mol·s) (Fig. 2(B)). This indicates that, rather than ^{3}CDOM*, CDOM is the source of $^{\bullet}$OH, which is less effective because of the scavenging effect of DOM on $^{\bullet}$OH. This effect is noticeable even under conditions with high DOC (Fabbri et al., 2023).

The photolysis constants shown in Table 2 were input into APEX software with $k_{^3CDOM^*, LOS}$ = 0.05 $k_{^3AQ2S^*, LOS}$ because, compared with ^{3}CDOM*, ^{3}AQ2S* has greater reactivity with pollutants (Calza et al., 2017). Figure 2(A) displays the half-life of LOS in relation to the DOC concentration (0–5 mg/L) and water depth (0–5 m). The half-life of LOS between 0 and 100 days increased as both the DOC and water depth increased. The results corroborated the subsequent persistence projections (Fig. 5). Direct photolysis, $CO_3^{\bullet-}$, and $^1O_2$ contributed the most to LOS photodegradation, whereas ^{3}CDOM* contributed almost nothing to LOS degradation, as predicted by APEX (Fig. 2(B)). This finding illustrates the complexity of natural aquatic environments, as the secondary apparent rate constants of $^{\bullet}$OH and ^{3}AQ2S* were not low in the experimental results. However, the contribution of $^{\bullet}$OH to LOS degradation was low in the model predictions, whereas ^{3}CDOM* contributed almost nothing.

Considering the presence of chlorine in surface waters receiving discharged wastewater effluents, LOS was observed via chlorination, solar irradiation, and solar/chlorine at pH 7.0 to evaluate the combined effects of solar irradiation and chlorination. Fig. 3 shows that LOS almost did not degrade in the solar irradiation system because of the low Φ_{LOS} = 1.10 × 10^{-6}. Both the chlorination and solar/chlorine systems exhibited similar performances for the first 10 min. However, over time, the solar/chlorine system showed higher degradation efficiency than chlorination alone. The degradation of LOS after 10 min was largely influenced by photolysis, which accelerated its transformation. The LOS solution (5.0 μmol/L) was degraded by approximately 70% in the solar/chlorine system at 80 min but only by 50% during chlorination with the same concentration of FAC. This indicates that, under the combined action of solar radiation and chlorine, reactive substances such as $^{\bullet}$OH, $CO_3^{\bullet-}$, and $^1O_2$ are produced in the system, and radicals improve the reaction performance (Young et al., 2018; Chen et al., 2023).

3.3 Transformation mechanisms of LOS in water

The transformation of LOS is achieved by oxidation, light, and radical reactions, especially at intermediate pH values (Heeb et al., 2014; Xu et al., 2018). To elucidate the transformation mechanisms, the TPs of LOS in chlorination systems with or without bromide ions and in solar/chlorine systems were determined via LC-HRMS. A total of 14 TPs of LOS were detected across these three processes (Table S2). Fragmentation analysis of the identified TPs was conducted using MS/MS scans to yield measured *m/z* values for LOS and TPs, which showed satisfactory consistency (Table S3). Structural analysis of LOS and its TPs was performed on the basis of the MS/MS data (Fig. 2), and the detailed secondary MS data of LOS are outlined in Text S5. In addition, considering the negligible degradation of LOS by direct solar photolysis, the solar irradiation system was not included in the product analysis.

Figure 4 illustrates the primary transformation mechanisms involved in LOS degradation across the three studied systems, including hydroxylation, hydrogen abstraction, halogen substitution, demethylation, ring opening, and hydrolysis. Extensive research on advanced oxidation processes for micropollutant degradation has revealed the formation of numerous hydroxylated compounds during treatment (Cruz-González et al., 2016; Arshad et al., 2020; Zaouak et al., 2021). In all the reactions, TP-420 was produced by aldolization; TP-334 was formed by ring cleavage; TP-251 and TP-252 were generated by denitration; and TP-206 was obtained by bond breaking and hydroxylation. TP-438 was detected in the

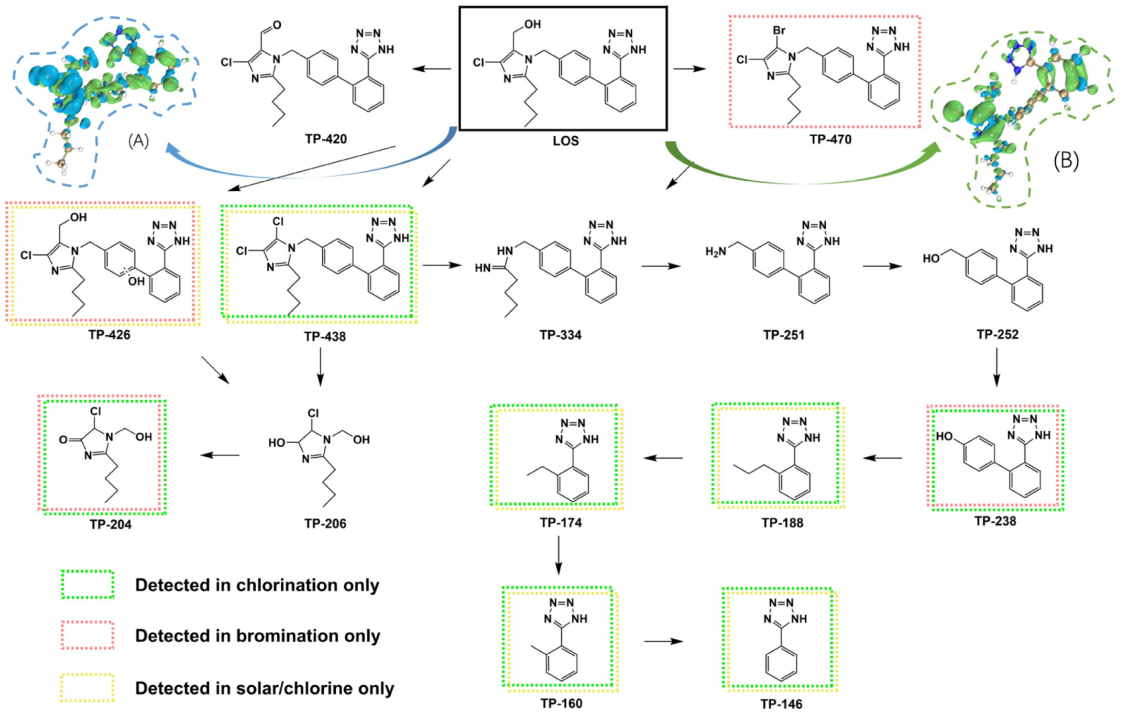

Fig. 4 The transformation mechanisms of LOS by chlorination, bromination, and solar/chlorine systems at pH 7.0 in phosphate buffer solution. (A) represents radical active sites, (B) indicates the electrophilic oxidant reactive sites. Conditions: $[LOS]_0$ = 5.0 μmol/L, $[FAC]_0$ = 100.0 μmol/L, [HOBr] = 5.0 μmol/L, xenon arc lamp intensity = 300 W/m^2.

chlorination and SSL/Cl systems and was generated by chlorine substitution. TP-238 and TP-204 were detected in the halogenation system, with the former being yielded by hydroxylation, whereas TP-204 was obtained by aldolization. Chlorination and bromination reactions yield corresponding halogenated products such as TP-470 and TP-426. Solar irradiation-induced radicals result in ring cleavage and carbon chain shortening to produce TP-188, TP-174, TP-160, and TP-146. Universal degradation processes, hydroxylation, and hydrogen abstraction are denoted by dotted lines due to uncertainty in the location of –OH groups during aromatic hydroxylation. Similar degradation pathways were detected in all three processes, with chlorination leading primarily to chlorine substitution and hydrogen abstraction, whereas TP-470 was exclusively present in bromination reactions owing to its oxidant specificity. The continuous demethylation of TP molecules was associated primarily with the solar/chlorine system. This process has been detected in chlorination experiments and could be due to radical action in certain solutions. TP-420, TP-438, TP-334, and TP-251 were detected in photo-electro-Fenton treatment, sonochemical treatment, electrochemical oxidation treatment, hydrogen peroxide treatment, and UV/PS (Fe^{2+}) treatment (Serna-Galvis et al., 2019; Martínez-Pachón et al., 2021; Ali et al., 2023), and TP-238 and TP-206 were found in •OH-based treatment (Zaouak et al., 2021), which is similar to our results.

To validate the accuracy of the transformation mechanisms, the Fukui function was used to describe the reactivity of LOS, whereas density functional theory (DFT) was utilized for geometric optimization. Gaussian 16 was used as the quantum chemistry software, with the wB97xd functional and def-TZVP basis set (Kaminský et al., 2013; De Vetta and Corral, 2019). Multiwfn was used for wave function analysis, and VMD was used for visualization (Shukla et al., 2020). As illustrated in Fig. 4(A), a broader distribution indicates higher reactivity with radicals. Figure 4(B) shows the reactivity of electrophilic reagents (e.g., the oxidizing agent employed in this research) with LOS, which is less active than radicals are, demonstrating the beneficial effect of solar radiation on chlorination. The figure shows that benzene rings and nitrogenous five-membered rings are more susceptible to attack by radicals and oxidants, whereas carbon chains are less reactive, supporting the ring-opening and halogen substitution mechanisms shown in Fig. 4. Notably, the reactivity of tetrazolium five-membered heterocycles is much lower than that of diazapentaheterocycles, which

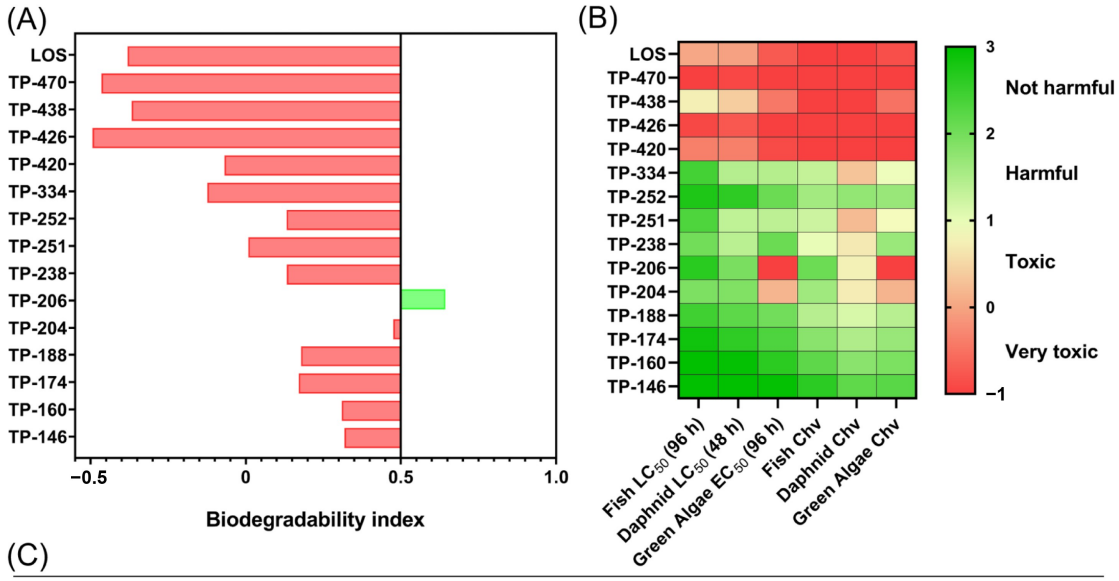

(C)

Comp.	Developmental toxicity	Ames mutagenicity	Estrogen receptor binding	Persistence	Bioaccumulation	Toxicity
LOS	–	–	√	P_3	B_1	T_3
TP-470	√	–	√	P_3	B_2	T_3
TP-438	–	–	–	P_3	B_1	T_3
TP-426	–	–	√	P_3	B_2	T_3
TP-420	–	–	√	P_3	B_1	T_3
TP-334	√	√	–	P_3	B_1	T_1
TP-252	√	–	√	P_3	B_1	T_1
TP-251	√	–	–	P_3	B_1	T_1
TP-238	√	–	√	P_3	B_1	T_2
TP-206	√	–	–	P_3	B_1	T_1
TP-204	√	–	–	P_3	B_1	T_1
TP-188	√	–	–	P_3	B_1	T_1
TP-174	√	–	–	P_3	B_1	T_1
TP-160	–	–	√	P_3	B_1	T_1
TP-146	–	–	–	P_3	B_1	T_1

Fig. 5 Prediction of (A) biodegradability index, (B) aquatic toxicity, (C) PBT, developmental toxicity, ames mutagenicity, and estrogen receptor binding of LOS and TPs generated in chlorination, bromination, and solar/chlorine at pH 7.0.

is likely due to the high activity of the functional groups attached to the latter.

3.4 Environmental risk evaluation of LOS and its TPs

Recent studies have suggested the risks of the TPs of micropollutants produced during oxidative water treatment and natural attenuation (Tian et al., 2021). To evaluate the impacts of chlorination, bromination, and photodegradation on the toxicity of LOS, initial assessments of the environmental characteristics of LOS and its degradation products were carried out using several well-known *in silico* prediction software programs, such as the EPI Suite™ and the online CompTox tool. Although the predicted results may not be completely correct, they can help assess the toxicity of TPs that cannot be subjected to practical experiments due to the difficulty of preparation and reduce laboratory costs. The efficiency of this digital estimation approach in determining the chemical and toxic properties of TPs of different substances (i.e., amoxicillin, sulfamethoxazole, ciprofloxacin, and diclofenac) in chlorination and photolysis processes has been demonstrated (Ortiz de García et al., 2014; Ofrydopoulou et al., 2021; Zhu et al., 2022).

Figure 5 presents the predicted biodegradability, acute/chronic toxicity, developmental toxicity, genotoxicity, and endocrine-disrupting effects, as well as the persistent, bio-accumulative, and toxic (PBT) characteristics of LOS and its various TPs. Nearly all of the TPs failed to exhibit any biodegradability (except TP-206), with a biodegradation index of < 0.5 (Fig. 5(A)). During the degradation process, the biodegradability of LOS tended to increase with increasing biodegradability of TP-406. The results confirmed that under the three treatments, LOS and its TPs still exhibited biodegradation resistance. Notably, the toxicity to fish, Daphnia, and green algae decreased after chlorination, bromination, and solar/chlorine treatment. The macromolecular TPs TP-470, TP-438, TP-426, and TP-420 were predicted to be highly toxic. TP-334 and TP-251 pose chronic risks to Daphnia, and TP-206 and TP-204 have toxic effects on green algae, which is attributed to the high toxicity of benzyl alcohol, imidazole, and aldehyde moieties to fish, Daphnia, and green algae; the toxicity of the aliphatic amine moiety to Daphnia; and the toxicity of the halo alcohol and haloacetamide moieties to green algae (Fig. 5(B)). In particular, TP-252, TP-238, TP-188, TP-176, TP-160, and TP-146 presented reduced toxicity (Fig. 5(B)). Research has shown that the TPs of LOS formed in the UV/H_2O_2 treatment at 240 min had effects on Daphnia. Risk assessment tools suggest that the combination of LOS with FAC or persulfate may result in heightened toxicity in the solution (Carpinteiro et al., 2019; Adams et al., 2021; Ioannidi et al., 2022), which was similar to the findings of our study. Developmental toxicity, genotoxicity, and endocrine-disrupting effects were predicted by CompTox software, with most TPs exhibiting developmental toxicity but not mutagenicity. Nearly half of the TPs were found to have endocrine-disrupting effects. Owing to the complexity of the endocrine-disrupting effects, EDC-Predictor was used to explore the specific effects (Fig. S9). The PBT properties of LOS and its TPs following different treatments are shown in Fig. 5(C).

4 Conclusions

This work presents in-depth insights into the degradation kinetics, reaction mechanisms, and environmental risks of LOS during chlorination, bromination, photolysis, and combined solar/chlorine treatment. At pH 5.0–8.0, the reactivity of bromination was greater than that of chlorination because of the contribution of BrO^- (i.e., at pH 7.0, $k_{app,\ HClO\ (LOS)}$ = 1.24 L/(mol·s), and $k_{app,\ HBrO\ (LOS)}$ = 6.68 × 10^4 L/(mol·s)). The photodegradation of LOS is dominated by $CO_3^{\bullet -}$ generation under low-DOC conditions and by direct photolysis and $^1O_2$ under high-DOC conditions. The half-life of LOS degradation in natural water was predicted to be 100 days at [DOC] = 5 mg/L and a water depth = 5.0 m. Furthermore, the reaction rate of LOS in the solar/chlorine system was greater than the rate observed under solar irradiation or chlorination alone. The major transformation mechanisms of LOS during degradation were hydroxylation, hydrogen abstraction, halogen substitution, demethylation, ring opening, and hydrolysis, and 14 TPs were detected in the three abovementioned systems. According to the *in silico* predictions, most of the TPs of LOS exhibited poor biodegradability, except for TP-206. Approximately half of the TPs caused acute/chronic toxicity to aquatic organisms to different degrees, along with developmental toxicity and endocrine-disrupting effects. These results indicated that the transport of LOS from chlorine-based disinfection units to sunlit freshwater may have undesired effects on aquatic ecosystems.

Conflict of Interests Mingbao Feng is a youth editorial board member of *Frontiers of Environmental Science & Engineering*. The authors declare that they have no known competing financial interests or personal relationships that might influence the work reported.

Acknowledgements This work was supported by the National Key R&D Program of China (No. 2023YFE0112100), the Natural Science Foundation of Xiamen (China) (No. 3502Z202373008), and the National Natural Science Foundation of China (Nos. 22476166 and 42376210).

Electronic Supplementary Material Supplementary material is available in the online version of this article at https://doi.org/10.1007/s11783-025-1968-9 and is accessible for authorized users.

References

Abdallah P, Deborde M, Dossier Berne F, Karpel Vel Leitner N (2015). Kinetics of chlorination of benzophenone-3 in the presence of bromide and ammonia. Environmental Science & Technology, 49(24): 14359–14367

Abdallah P, Dossier-Berne F, Karpel Vel Leitner N, Deborde M (2021). Methylparaben chlorination in the presence of bromide ions and ammonia: kinetic study and modeling. Environmental Science and Pollution Research International, 28(24): 31256–31267

Acero J L, Benitez F J, Real F J, Roldan G, Rodriguez E (2013). Chlorination and bromination kinetics of emerging contaminants in aqueous systems. Chemical Engineering Journal, 219: 43–50

Adams E, Neves B B, Prola L D T, De Liz M V, Martins L R R, Ramsdorf W A, De Freitas A M (2021). Ecotoxicity and

genotoxicity assessment of losartan after UV/H_2O_2 and UVC/photolysis treatments. Environmental Science and Pollution Research International, 28(19): 23812–23821

Ali I, Barros de Souza A, Liu Z, Cabooter D, Katsaounis A, De Laet S, Van Eyck K, Dewil R (2023). Improving the removal of losartan, irbesartan and their transformation products through in situ produced hydrogen peroxide in electrochemical oxidation processes. Journal of Water Process Engineering, 55: 104133

Arshad R, Bokhari T H, Khosa K K, Bhatti I A, Munir M, Iqbal M, Iqbal D N, Khan M I, Nazir A (2020). Gamma radiation induced degradation of anthraquinone Reactive Blue-19 dye using hydrogen peroxide as oxidizing agent. Radiation Physics and Chemistry, 168: 108637

Baeza C, Knappe D R U (2011). Transformation kinetics of biochemically active compounds in low-pressure UV Photolysis and UV/H_2O_2 advanced oxidation processes. Water Research, 45(15): 4531–4543

Becker R W, Cardoso R M, Dallegrave A, Ruiz-Padillo A, Sirtori C (2023). Quantification of pharmaceuticals in hospital effluent: weighted ranking of environmental risk using a fuzzy hybrid multicriteria method. Chemosphere, 338: 139368

Bodrato M, Vione D (2014). APEX (aqueous photochemistry of environmentally occurring xenobiotics): a free software tool to predict the kinetics of photochemical processes in surface waters. Environmental Science. Processes & Impacts, 16(4): 732–740

Calza P, Noè G, Fabbri D, Santoro V, Minero C, Vione D, Medana C (2017). Photoinduced transformation of pyridinium-based ionic liquids, and implications for their photochemical behavior in surface waters. Water Research, 122: 194–206

Carena L, Vione D, Minella M, Canonica S, Schönenberger U (2022). Inhibition by phenolic antioxidants of the degradation of aromatic amines and sulfadiazine by the carbonate radical ($CO_3^{\bullet-}$). Water Research, 209: 117867

Carpinteiro I, Castro G, Rodríguez I, Cela R (2019). Free chlorine reactions of angiotensin II receptor antagonists: kinetics study, transformation products elucidation and *in-silico* ecotoxicity assessment. Science of the Total Environment, 647: 1000–1010

Chen T, Taylor-Edmonds L, Andrews S, Hofmann R (2023). Kinetics of hydrogen peroxide quenching following UV/H_2O_2 advanced oxidation by thiosulfate, bisulfite, and chlorine in drinking water treatment. Frontiers of Environmental Science & Engineering, 17(12): 147

Cruz-González G, Rivas-Ortiz I B, González-Labrada K, Rapado-Paneque M, Chávez-Ardanza A, Nuevas-Paz L, Jáuregui-Haza U J (2016). Improving degradation of paracetamol by integrating gamma radiation and Fenton processes. Journal of Environmental Science and Health. Part A, Toxic/Hazardous Substances & Environmental Engineering, 51(12): 997–1002

De Vetta M, Corral I (2019). Insight into the optical properties of meso-pentafluorophenyl(PFP)-BODIPY: an attractive platform for functionalization of BODIPY dyes. Computational & Theoretical Chemistry, 1150: 110–120

Fabbri D, Carena L, Bertone D, Brigante M, Passananti M, Vione D (2023). Assessing the photodegradation potential of compounds derived from the photoinduced weathering of polystyrene in water. Science of the Total Environment, 876: 162729

Hao Z, Ma J, Miao C, Song Y, Lian L, Yan S, Song W (2020). Carbonate radical oxidation of ccylindrospermopsin (*Cyanotoxin*): kinetic studies and mechanistic consideration. Environmental Science & Technology, 54(16): 10118–10127

Heeb M B, Criquet J, Zimmermann-Steffens S G, Von Gunten U (2014). Oxidative treatment of bromide-containing waters: formation of bromine and its reactions with inorganic and organic compounds: a critical review. Water Research, 48: 15–42

Hu C Y, Zhang J C, Lin Y L, Ren S C, Zhu Y Y, Xiong C, Wang Q B (2021). Degradation kinetics of prometryn and formation of disinfection by-products during chlorination. Chemosphere, 276: 130089

Hua Z, Guo K, Kong X, Lin S, Wu Z, Wang L, Huang H, Fang J (2019). PPCP degradation and DBP formation in the solar/free chlorine system: effects of pH and dissolved oxygen. Water Research, 150: 77–85

Ioannidi A, Arvaniti O S, Nika M C, Aalizadeh R, Thomaidis N S, Mantzavinos D, Frontistis Z (2022). Removal of drug losartan in environmental aquatic matrices by heat-activated persulfate: Kinetics, transformation products and synergistic effects. Chemosphere, 287: 131952

Jiang J Q, Lloyd B (2002). Progress in the development and use of ferrate(VI) salt as an oxidant and coagulant for water and wastewater treatment. Water Research, 36(6): 1397–1408

Kaminský J, Buděšínský M, Taubert S, Bouř P, Straka M (2013). Fullerene C70 characterization by ^{13}C NMR and the importance of the solvent and dynamics in spectral simulations. Physical Chemistry Chemical Physics, 15(23): 9223–9230

Lai W W P, Chen K L, Lin A Y C (2020). Solar photodegradation of the UV filter 4-methylbenzylidene camphor in the presence of free chlorine. Science of the Total Environment, 722: 137860

Lastre-Acosta A M, Barberato B, Parizi M P S, Teixeira A C S C (2019). Direct and indirect photolysis of the antibiotic enoxacin: kinetics of oxidation by reactive photo-induced species and simulations. Environmental Science and Pollution Research International, 26(5): 4337–4347

Lee W, Lee Y, Allard S, Ra J, Han S, Lee Y (2020). Mechanistic and kinetic understanding of the UV_{254} photolysis of chlorine and bromine species in water and formation of oxyhalides. Environmental Science & Technology, 54(18): 11546–11555

Lei H, Mariñas B J, Minear R A (2004). Bromamine decomposition kinetics in aqueous solutions. Environmental Science & Technology, 38(7): 2111–2119

Li W, Liu K, Min Z, Li J, Zhang M, Korshin G V, Han J (2023). Transformation of macrolide antibiotics during chlorination process: kinetics, degradation products, and comprehensive toxicity evaluation. Science of the Total Environment, 858: 159800

Li W, Tanumihardja J, Masuyama T, Korshin G (2015). Examination of the kinetics of degradation of the antineoplastic

drug 5-fluorouracil by chlorine and bromine. Journal of Hazardous Materials, 282: 125–132

Ling L, Sun J, Fang J, Shang C (2016). Kinetics and mechanisms of degradation of chloroacetonitriles by the UV/H_2O_2 process. Water Research, 99: 209–215

Liu J, Zhang X, Li Y, Li W, Hang C, Sharma V K (2019). Phototransformation of halophenolic disinfection byproducts in receiving seawater: kinetics, products, and toxicity. Water Research, 150: 68–76

Liu Q T, Williams H E (2007). Kinetics and degradation products for direct photolysis of β-blockers in water. Environmental Science & Technology, 41(3): 803–810

Martínez-Pachón D, Serna-Galvis E A, Ibañez M, Hernández F, Ávila-Torres Y, Torres-Palma R A, Moncayo-Lasso A (2021). Treatment of two sartan antihypertensives in water by photo-electro-Fenton using BDD anodes: degradation kinetics, theoretical analyses, primary transformations and matrix effects. Chemosphere, 270: 129491

Meyer M F, Powers S M, Hampton S E (2019). An evidence synthesis of pharmaceuticals and personal care products (PPCPs) in the environment: imbalances among compounds, sewage treatment techniques, and ecosystem types. Environmental Science & Technology, 53(22): 12961–12973

Ofrydopoulou A, Evgenidou E, Nannou C, Vasquez M I, Lambropoulou D (2021). Exploring the phototransformation and assessing the *in vitro* and *in silico* toxicity of a mixture of pharmaceuticals susceptible to photolysis. Science of the Total Environment, 756: 144079

Ofrydopoulou A, Nannou C, Evgenidou E, Christodoulou A, Lambropoulou D (2022). Assessment of a wide array of organic micropollutants of emerging concern in wastewater treatment plants in Greece: occurrence, removals, mass loading and potential risks. Science of the Total Environment, 802: 149860

Oosterhuis M, Sacher F, ter Laak T L (2013). Prediction of concentration levels of metformin and other high consumption pharmaceuticals in wastewater and regional surface water based on sales data. Science of the Total Environment, 442: 380–388

Ortiz de García S A, Pinto Pinto G, García-Encina P A, Irusta-Mata R (2014). Ecotoxicity and environmental risk assessment of pharmaceuticals and personal care products in aquatic environments and wastewater treatment plants. Ecotoxicology, 23(8): 1517–1533

Ouyang W Y, Wang W L, Zhang Y L, Cai H Y, Wu Q Y (2023). VUV/UV oxidation performance for the elimination of recalcitrant aldehydes in water and its variation along the light-path. Water Research, 228: 119390

Pozdnyakov I P, Tyutereva Y E, Parkhats M V, Grivin V P, Fang Y, Liu L, Wan D, Luo F, Chen Y (2020). Mechanistic investigation of humic substances assisted photodegradation of imipramine under simulated sunlight. Science of the Total Environment, 738: 140298

Qin L, Lin Y L, Xu B, Hu C Y, Tian F X, Zhang T Y, Zhu W Q, Huang H, Gao N Y (2014). Kinetic models and pathways of ronidazole degradation by chlorination, UV irradiation and UV/chlorine processes. Water Research, 65: 271–281

Rose M R, Lau S S, Prasse C, Sivey J D (2020). Exotic electrophiles in chlorinated and chloraminated water: when conventional kinetic models and reaction pathways fall short. Environmental Science & Technology Letters, 7(6): 360–370

Rosenfeldt E J, Linden K G (2004). Degradation of endocrine disrupting chemicals bisphenol A, ethinyl estradiol, and estradiol during UV photolysis and advanced oxidation processes. Environmental Science & Technology, 38(20): 5476–5483

Roveri V, Guimarães L L, Toma W, Correia A T (2020). Occurrence and ecological risk assessment of pharmaceuticals and cocaine in a beach area of Guarujá, São Paulo State, Brazil, under the influence of urban surface runoff. Environmental Science and Pollution Research International, 27(36): 45063–45075

Russo D, Cochran K H, Westerman D, Li Puma G, Marotta R, Andreozzi R, Richardson S D (2020). Ultrafast photodegradation of isoxazole and isothiazolinones by UV_{254} and UV_{254}/H_2O_2 photolysis in a microcapillary reactor. Water Research, 169: 115203

Serna-Galvis E A, Isaza-Pineda L, Moncayo-Lasso A, Hernández F, Ibáñez M, Torres-Palma R A (2019). Comparative degradation of two highly consumed antihypertensives in water by sonochemical process. Determination of the reaction zone, primary degradation products and theoretical calculations on the oxidative process. Ultrasonics Sonochemistry, 58: 104635

Shang M, Kong Y, Yang Z, Cheng R, Zheng X, Liu Y, Chen T (2023). Removal of virus aerosols by the combination of filtration and UV-C irradiation. Frontiers of Environmental Science & Engineering, 17(3): 27

Shu Z, Li C, Belosevic M, Bolton J R, El-Din M G (2014). Application of a solar UV/chlorine advanced oxidation process to oil sands process-affected water remediation. Environmental Science & Technology, 48(16): 9692–9701

Shukla S, Srivastava A, Kumar P, Tandon P, Maurya R, Singh R B (2020). Vibrational spectroscopic, NBO, AIM, and multiwfn study of tectorigenin: a DFT approach. Journal of Molecular Structure, 1217: 128443

Soares D F, Faria A M, Rosa A H (2017). Análise de risco de contaminação de águas subterrâneas por resíduos de agrotóxicos no município de Campo Novo do Parecis (MT), Brasil. Engenharia Sanitaria e Ambiental, 22: 277–284

Tian Z, Zhao H, Peter K T, Gonzalez M, Wetzel J, Wu C, Hu X, Prat J, Mudrock E, Hettinger R, et al. (2021). A ubiquitous tire rubber-derived chemical induces acute mortality in coho salmon. Science, 371(6525): 185–189

Wang W L, Jing Z B, Zhang Y L, Wu Q Y, Drewes J E, Lee M Y, Hübner U (2024). Assessing the chemical-free oxidation of trace organic chemicals by VUV/UV as an alternative to conventional UV/H_2O_2. Environmental Science & Technology, 58(16): 7113–7123

Wu Z, Fang J, Xiang Y, Shang C, Li X, Meng F, Yang X (2016). Roles of reactive chlorine species in trimethoprim degradation in

the UV/chlorine process: kinetics and transformation pathways. Water Research, 104: 272–282

Xu B, Deng L, Zhang S, Luo W, Hu J, Tan C, Singh R P (2023). Analysis of degradation kinetic modeling and mechanism of chlorinated-halonitromethanes under UV/monochloramine treatment. Environmental Pollution, 319: 120972

Xu X, Xiao R, Dionysiou D D, Spinney R, Fu T, Li Q, Wang Z, Wang D, Wei Z (2018). Kinetics and mechanisms of the formation of chlorinated and oxygenated polycyclic aromatic hydrocarbons during chlorination. Chemical Engineering Journal, 351: 248–257

Young T R, Li W, Guo A, Korshin G V, Dodd M C (2018). Characterization of disinfection byproduct formation and associated changes to dissolved organic matter during solar photolysis of free available chlorine. Water Research, 146: 318–327

Zaouak A, Noomen A, Jelassi H (2021). Degradation mechanism of losartan in aqueous solutions under the effect of gamma radiation. Radiation Physics and Chemistry, 184: 109435

Zhang T, Huang C H (2020). Modeling the kinetics of UV/peracetic acid advanced oxidation process. Environmental Science & Technology, 54(12): 7579–7590

Zhou Y, Chen C, Guo K, Wu Z, Wang L, Hua Z, Fang J (2020). Kinetics and pathways of the degradation of PPCPs by carbonate radicals in advanced oxidation processes. Water Research, 185: 116231

Zhu J, Yang L, Wang M, Zhang Q, Zhang Y, Li Y (2022). The influence of bromide and iodide ions on the sulfamethoxazole (SMX) halogenation during chlorination. Science of the Total Environment, 848: 157687